batteries

MDPI

Article

Chemically Active LiH_2PO_4 Interphase Precursor Enables Self-Limited Interface Stabilization in Sulfide-Based All-Solid-State Batteries

Youngmin Lee [1,2], Eun Chan Heo [3], Yong Joon Park [3,*] and Dongwook Shin [1,2,*]

[1] Division of Materials Science & Engineering, Hanyang University, Seongdong-gu, Seoul 04763, Republic of Korea; ymlee@solivis.com
[2] Solivis Inc., 30 Misagangbyeonjungang-ro, 31beon-gil, Hanam-si 12939, Gyeonggi-do, Republic of Korea
[3] Department of Advanced Materials Engineering, Graduate School Kyonggi University, 154-42, Gwanggyosan-ro, Yeongtong-gu, Suwon-si 16227, Gyeonggi-do, Republic of Korea
* Correspondence: yjpark2006@kyonggi.ac.kr (Y.J.P.); dwshin@hanyang.ac.kr (D.S.)

Abstract

The commercialization of sulfide-based all-solid-state batteries (ASSBs) is severely limited by the interfacial degradation between layered oxide cathodes and sulfide solid electrolytes, resulting in electrolyte decomposition, impedance growth, and rapid capacity fading. Herein, we propose lithium dihydrogen phosphate (LiH_2PO_4, LDP) as a low-cost polyanionic interphase precursor to regulate the cathode–electrolyte interface. A uniform LDP coating was deposited onto polycrystalline NCM622 particles, producing a continuous 40-nm-thick phosphate layer. Although the LDP-coated electrode exhibited a higher initial interfacial resistance than the bare cathode, electrochemical analyses revealed a capacity retention of 94.1% after 100 cycles, compared with 73.9% for the uncoated electrode. X-ray photoelectron spectroscopy demonstrated that LiH_2PO_4 is not chemically inert toward Li_6PS_5Cl but undergoes a controlled initial reaction with sulfur-deficient species to generate a phosphate-rich artificial interphase while suppressing the unstable P–$[S]_n$–P species. This interphase rapidly reaches chemical equilibrium, suppressing sulfur precipitation, SO_x formation, and subsequent electrolyte decomposition. Cross-sectional STEM–EDS and focused ion beam analyses revealed that the artificial phosphate interphase inhibited elemental interdiffusion, suppressed chemical mixing, and preserved mechanical contact during prolonged cycling. These findings demonstrate that the electrochemical penalty associated with the initial formation of the LDP interphase represents the necessary cost of constructing a chemically stable interface rather than a degradation process. This study introduces a new interfacial design strategy based on chemically active sacrificial interphase precursors, providing an alternative to conventional inert oxide coatings for realizing long-term stable sulfide-based all-solid-state batteries.

Keywords: all-solid-state batteries; sulfide electrolyte; cathode; surface modification; interphase precursor

Check for updates

Academic Editor: Jinkui Feng

Received: 31 July 2026
Revised: 24 August 2026
Accepted: 24 August 2026
Published: 26 August 2026

Copyright: © 2026 by the authors. Licensee MDPI, Basel, Switzerland. This article is an open access article distributed under the terms and conditions of the Creative Commons Attribution (CC BY) license.

1. Introduction

All-solid-state lithium batteries (ASSBs) are promising next-generation electrochemical energy-storage technologies, with the potential to deliver high energy density, superior safety, and extended service life beyond those achievable with conventional lithium-ion batteries containing flammable organic liquid electrolytes [1–5]. Among the various classes

of solid electrolytes, sulfide-based electrolytes have attracted particular attention because of their exceptionally high lithium-ion conductivity (>10^{-3} S cm^{-1}), excellent mechanical deformability, and ability to establish intimate solid–solid contact with electrode materials under relatively low stack pressures [6–11]. These unique characteristics make sulfide electrolytes highly attractive for practical ASSBs that employ high-capacity layered oxide cathodes.

Despite these advantages, the commercialization of sulfide ASSBs is impeded by the severe interfacial instability at the oxide cathode–solid electrolyte interface [12–16]. The large chemical potential mismatch between oxide cathodes and sulfide electrolytes and their fundamentally different thermodynamic stability windows drive spontaneous interfacial reactions even before electrochemical cycling. These reactions produce electronically insulating and ionically resistive decomposition products, including lithium sulfide (Li_2S), phosphorus sulfides (P_xS_y), transition-metal sulfides (MS_x), and phosphate species (MPO_4), which continuously accumulate during repeated cycling. Consequently, lithium-ion transport is progressively hindered, charge-transfer resistance increases, and electrochemical polarization is aggravated, ultimately leading to rapid capacity fading. Moreover, space-charge layer formation and chemo-mechanical contact degradation further accelerate interfacial deterioration. Interface engineering is therefore one of the most critical prerequisites for realizing high-performance sulfide ASSBs.

Surface passivation of oxide cathodes has therefore become one of the most extensively investigated strategies for suppressing interfacial degradation [17–23]. However, next-generation cathode passivation layers must satisfy far more stringent requirements than merely suppressing interfacial reactions. Existing coating materials are predominantly based on Nb-, Ta-, or Zr-containing oxides [20–23], which inevitably increase material costs and are therefore less attractive for large-scale battery manufacturing. Many oxide coatings exhibit only moderate electrochemical stability under increasingly demanding high-voltage operating conditions, while their chemical compatibility with sulfide electrolytes is far from ideal [24–26]. Therefore, future interface materials should simultaneously provide broad electrochemical stability, excellent chemical compatibility with sulfide electrolytes, low interfacial resistance, facile Li-ion transport, and scalable and low-cost processing. Achieving these attributes using a single coating material remains a significant challenge.

Polyanionic lithium compounds have emerged as attractive alternatives; their strong covalent polyanion frameworks have substantially higher oxidative stability than conventional simple oxides [14,15,27]. Lithium dihydrogen phosphate (LiH_2PO_4, LDP) is a particularly intriguing example. Although it has only been applied a few times to cathodes for lithium battery systems using liquid electrolytes [28,29], it has yet to be extensively studied for use in cathode coatings with sulfide electrolytes. Unlike transition-metal-containing coating materials, LDP is composed exclusively of earth-abundant and inexpensive elements, offering significant economic advantages for large-scale commercialization. More importantly, its phosphate framework comprises highly stable P–O covalent bonds, which are expected to provide excellent oxidative stability and favorable chemical compatibility with sulfide electrolytes [28–30]. First-principles calculations predict that phosphate-based compounds have wide electrochemical stability windows, along with intrinsically low interfacial reactivity toward sulfide electrolytes [27]. Despite its promising characteristics, LiH_2PO_4 has received little attention as a cathode passivation material for all-solid-state cells. There has been no systematic investigation into its ability to simultaneously suppress sulfide electrolyte decomposition, preserve rapid Li-ion transport, and stabilize the cathode–electrolyte interface.

Herein, we propose LiH_2PO_4 as a new low-cost polyanionic passivation layer for sulfide-based ASSBs and demonstrate its effectiveness using polycrystalline $LiNi_{0.6}Co_{0.2}Mn_{0.2}O_2$

(NCM622) cathodes. A uniform LDP coating was fabricated using a scalable spray-drying process, providing a simple and industrially viable route for large-area surface modification. We hypothesize that the phosphate-rich interfacial layer not only suppresses undesirable chemical reactions between the oxide cathode and sulfide electrolyte but also forms a chemically compatible interface that minimizes interfacial resistance while preserving efficient lithium-ion transport. To validate this hypothesis, the interfacial chemistry, electrochemical behavior, and degradation mechanisms of the LDP-coated cathodes were systematically investigated through complementary structural, chemical, and electrochemical characterization techniques, including scanning electron microscopy (SEM), transmission electron microscopy (TEM), X-ray photoelectron spectroscopy (XPS), and electrochemical impedance spectroscopy (EIS). Figure 1 illustrates the expected effects of the LDP coating. This study establishes LiH_2PO_4 as a promising low-cost phosphate-based interface material and provides new principles for designing economically viable polyanionic coatings that can simultaneously achieve interfacial stability, fast ion transport, and long-term durability in next-generation sulfide ASSBs.

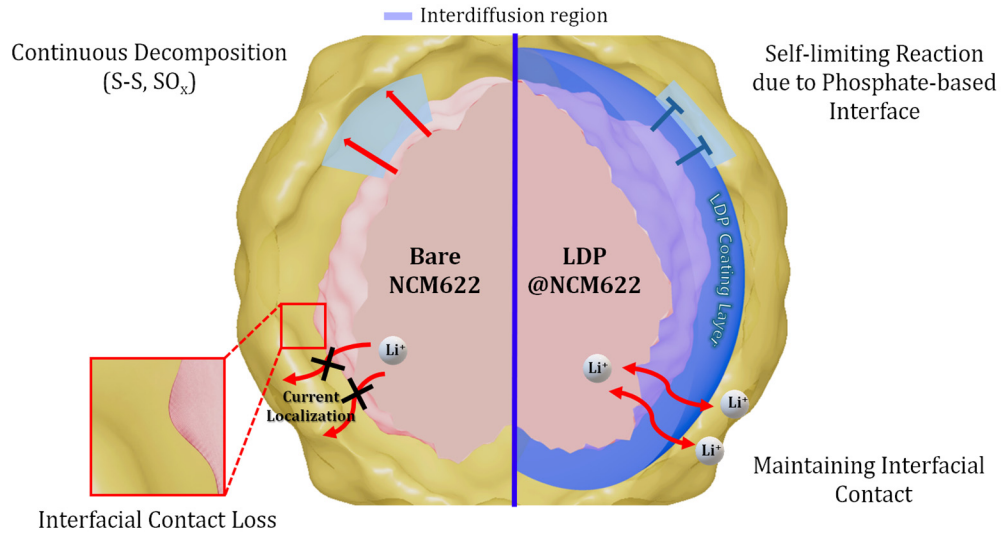


Figure 1. Schematic of the proposed interfacial stabilization mechanism induced by the LiH_2PO_4 (LDP) coating.

2. Experimental Section

2.1. Synthesis of LiH_2PO_4 and Cathode Coating

To identify an appropriate precursor solution for LiH_2PO_4 (LDP) coating, preliminary synthesis experiments were conducted using different lithium sources and solvents. An ideal coating precursor should be completely soluble, without precipitating or causing undesirable side reactions. LDP was therefore synthesized via three different routes: (i) Lithium hydroxide monohydrate ($LiOH{\cdot}H_2O$, Sigma-Aldrich, Korea) and phosphoric acid (H_3PO_4, Sigma-Aldrich, Korea) were separately dissolved in ethanol, and the resulting solutions were subsequently combined under vigorous stirring. The solvent was then evaporated under continuous stirring, followed by drying at 60 °C to remove residual solvent. (ii) Lithium hydroxide monohydrate ($LiOH{\cdot}H_2O$) and phosphoric acid (H_3PO_4) were sequentially dissolved in deionized water under vigorous stirring. The resulting solution was subsequently dried at 60 °C to completely remove the solvent. (iii) Anhydrous lithium hydroxide (LiOH) and phosphoric acid (H_3PO_4) were sequentially dissolved in deionized water under vigorous stirring. The resulting solution was subsequently dried at 60 °C to completely remove the solvent. Among these approaches, the ethanol-based

precursor showed the most favorable solution stability and coating processability and was therefore selected for subsequent coating experiments.

Commercial polycrystalline $LiNi_{0.6}Co_{0.2}Mn_{0.2}O_2$ (NCM622; Thermo Fisher Scientific) was used as the active cathode material. The LDP precursor solution was mixed with NCM622 to achieve an LDP loading of 1 wt.%, and the total suspension volume was adjusted to 200 mL using ethanol. Surface coating was performed using a laboratory-scale spray dryer (Mini Spray Dryer B-290, Büchi). The inlet temperature was maintained at 150 °C, the aspirator was operated at 100%, and the precursor suspension was continuously supplied at a feed rate of 6.6 mL min^{-1}. The collected powders were subsequently dried under vacuum at 80 °C for more than 12 h to ensure complete removal of the residual solvent. Hereinafter, the resulting material is referred to as LDP@NCM622. For a detailed structural characterization of the coating phase, an additional sample containing 10 wt% LDP was prepared using an identical procedure.

2.2. Material Characterization

The crystal structures of the pristine LDP and coated cathode materials were characterized by X-ray diffraction (XRD; SmartLab, Rigaku, Japan) using an airtight Kapton film sample holder. Diffraction patterns were collected over a 2θ range of 10–60° using monochromatized Cu-K_α radiation (λ = 1.5406 Å) with a scanning rate of 1° min^{-1}. The surface morphology and elemental distribution were examined using a field-emission scanning electron microscope (FE-SEM, Apreo 2, Thermo Fisher Scientific) equipped with an energy-dispersive X-ray spectroscopy (EDS) detector (EDAX, AMETEK). FE-SEM images were acquired in secondary electron (SE) and backscattered electron (BSE) modes at an accelerating voltage of 1.0 kV and a probe current of 0.10 nA. High-resolution microstructural analyses were performed using TEM and scanning transmission electron microscopy coupled with EDS (STEM–EDS, Spectra Ultra, Thermo Fisher Scientific) operated at an accelerating voltage of 300 kV. The cross-sectional TEM specimens were prepared using focused ion beam (FIB; Helios G5; Thermo Fisher Scientific). The surface chemical composition and electronic states of the cathode materials before and after electrochemical cycling were analyzed by XPS (XPS; Nexsa G2, Thermo Fisher Scientific) using a vacuum transfer holder and a microfocused Al Kα X-ray source with a spot size of 400 μm.

2.3. Electrochemical Measurements

All-solid-state cells were assembled using a Li–In alloy as the counter/reference electrode and a Li_6PS_5Cl argyrodite solid electrolyte (Solivis Inc.; median particle size, D_{50} = 3.8 μm) as the separator electrolyte. For cell fabrication, 0.015 g of the cathode composite, 0.15 g of the solid electrolyte separator, and 0.03 g of Li–In alloy powder were used, and the assembled cell was subsequently compressed under a pressure of 45 MPa. The Li–In alloy was prepared at a Li-to-In weight ratio of 2.5:97.5; specifically, 0.025 g of Li and 0.975 g of In were used to prepare 1 g of the alloy. The components were homogenized using a planetary centrifugal mixer (Thinky) at 1500 rpm for 1 min to obtain a uniformly mixed Li–In alloy powder. Galvanostatic charge–discharge measurements were performed using a WonATech battery cycler at a current corresponding to 0.22 C based on the theoretical capacity of NCM622 (200 mAh g^{-1}). Long-term cycling performance was evaluated over 100 cycles. To monitor the evolution of the interfacial degradation during cycling, EIS was performed after the 51st and 101st charge cycles.

3. Results and Discussion

The phase purity of LiH_2PO_4 (LDP) synthesized via the three routes described in Section 2 was examined by X-ray diffraction. As shown in Figure S1, all three synthe-

sis routes successfully produced crystalline LDP. However, the simultaneous addition of lithium and phosphate precursors to either ethanol or deionized water resulted in immediate precipitation; this prevented the preparation of a homogeneous precursor solution suitable for coating. Accordingly, the ethanol-based synthesis route was selected for subsequent fabrication of the LiH_2PO_4-coated cathodes.

In sulfide-based ASSBs, the effectiveness of an artificial passivation layer depends not only on its intrinsic chemical stability but also on the uniformity and morphology with which it is formed on the cathode surface. Therefore, prior to electrochemical evaluation, the structural characteristics of the LDP coating were systematically investigated. Figure S2 presents a comparison of the XRD patterns of pristine LiH_2PO_4 (LDP), bare NCM622, and LDP-coated NCM622 prepared with coating loadings of 1 and 10 wt.%. For the 1 wt.% coated sample (hereinafter denoted by LDP@NCM622), no discernible peak shift or change in the characteristic reflections of layered NCM622 was observed. In particular, the well-resolved splitting of the (006)/(102) and (108)/(110) reflections remained unchanged, confirming that the layered α-$NaFeO_2$ structure was fully preserved after the coating process. Conventional oxide coatings generally require post-annealing at temperatures above 500–700 °C to crystallize the coating layer, often resulting in oxygen loss or structural degradation in Ni-rich layered oxides. However, the present LDP coating was formed through a solution-assisted spray-drying process without any high-temperature crystallization treatment. Consequently, the bulk crystal structure of NCM622 remained unaffected, indicating that any subsequent improvement in the electrochemical performance originated from interfacial engineering rather than bulk structural modification. Although the diffraction peaks of LiH (PO) were difficult to distinguish in the 1 wt.% sample because of the low coating content, characteristic LDP reflections became clearly visible in the 10 wt.% sample. This confirmed that LiH_2PO_4 remained chemically stable throughout the spray-drying process without decomposing into secondary phosphate phases.

Figure 2 shows the morphology of the coated particles examined by SEM. As shown in Figure 2a,b, the secondary particle morphology of NCM622 remains essentially unchanged after spray drying, with no evidence of particle fracture, aggregation, or surface etching. This demonstrates that the coating process was sufficiently mild to preserve the structural integrity of commercial polycrystalline cathode particles. This preservation is particularly important, because secondary particle cracking provides preferential pathways for electrolyte penetration and accelerates intergranular degradation during cycling.

The effectiveness of the coating process was further demonstrated by elemental mapping (Figure 2c–f). In addition to the uniform distributions of Ni and Co, phosphorus, which originated exclusively from LiH_2PO_4, was homogeneously distributed over the entire particle surface. The superposition of the phosphorus elemental map with the secondary electron image clearly shows that phosphorus continuously surrounds individual secondary particles rather than forming isolated phosphate agglomerates. Such conformal coverage is essential for sulfide-based ASSBs because discontinuous coatings leave locally exposed cathode surfaces. These surfaces are susceptible to direct contact with sulfide electrolytes, which may initiate localized interfacial decomposition propagating throughout the electrode. Therefore, the highly uniform phosphorus distribution suggests that the spray-drying process effectively establishes a continuous artificial interface capable of suppressing spatially heterogeneous degradation while promoting homogeneous lithium-ion transport.

The nanoscale characteristics of the coating layer were further investigated using HAADF-STEM and high-resolution TEM (Figure 2g–j). HAADF elemental mapping revealed that phosphorus was confined exclusively to the outer surface of the primary particles, whereas Ni remained localized within the layered oxide interior. This comple-

mentary elemental distribution provides direct evidence that LiH_2PO_4 forms a genuine surface coating without diffusing into the bulk lattice of NCM622. High-resolution TEM further revealed a continuous coating layer with an average thickness of approximately 40 nm uniformly covering the primary particle surface (Figure 2i,j).

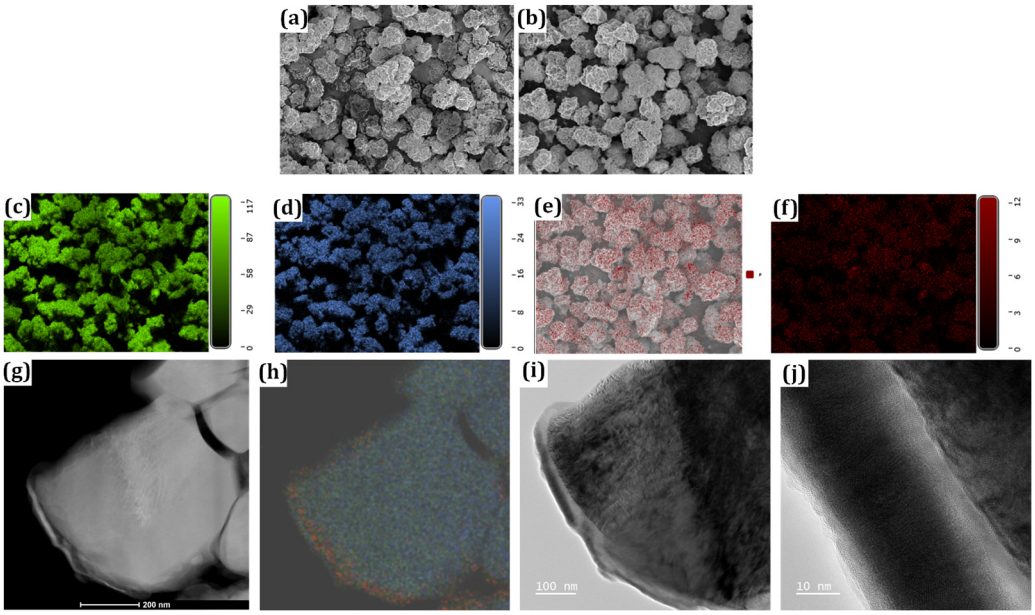


Figure 2. Structural and morphological characterizations of LDP@NCM622. (**a**,**b**) SEM images of bare NCM622 and LDP@NCM622. (**c**–**f**) SEM–EDS elemental mapping images of (**c**) Ni (BSE mode), (**d**) Co (BSE mode), (**e**) P (BSE mode), and (**f**) P (SE mode), demonstrating the uniform distribution of the LDP coating. (**g**) HAADF-STEM image and (**h**) corresponding STEM–EDS elemental mapping of Ni and P. (**i**,**j**) Low- and high-magnification TEM images showing the formation of a uniform LiH_2PO_4 coating layer with an average thickness of approximately 40 nm.

At first glance, this coating thickness appears to be substantially greater than that of conventional oxide passivation layers, which are typically only a few nanometers thick. However, the present coating was not intended to function as a physically inert diffusion barrier. Instead, as discussed in the following sections, the LiH_2PO_4 layer serves as a chemically active precursor that undergoes controlled interfacial reactions with the sulfide electrolyte during the initial electrochemical activation, thereby generating a chemically stable phosphate-rich interphase.

Following the formation of a uniform LDP coating on the cathode surface, the effectiveness of this artificial phosphate layer in regulating the electrochemical behavior of the cathode–electrolyte interface was investigated. Figures 3a and S3 present comparisons of the differential capacity (dQ/dV) profiles of bare NCM622 and LDP@NCM622 during the initial charge–discharge cycle. The bare electrode exhibits sharp oxidation and reduction peaks with a relatively small voltage polarization, indicative of facile charge transfer during the initial cycle. In contrast, the LDP-coated electrode displays broader redox peaks along with increased separation between the anodic and cathodic peaks, reflecting the additional kinetic barrier introduced by the phosphate layer. This behavior is attributed to the coating layer, which increases the initial lithium-ion diffusion pathway, and consequently, the interfacial impedance. A more important feature is the emergence of an additional reaction near 3.7 V in the bare electrode, which is absent in LDP@NCM622. Because this feature cannot be assigned to the intrinsic phase transitions of layered NCM622, it is attributed to parasitic interfacial reactions between the oxide cathode and sulfide electrolyte. Its complete suppression after the LDP coating indicates that the phosphate layer fundamen-

tally altered the initial interfacial reaction pathway. Rather than allowing direct electrolyte decomposition, the LDP coating is expected to promote the formation of a chemically stable phosphate-rich interphase during initial electrochemical activation.

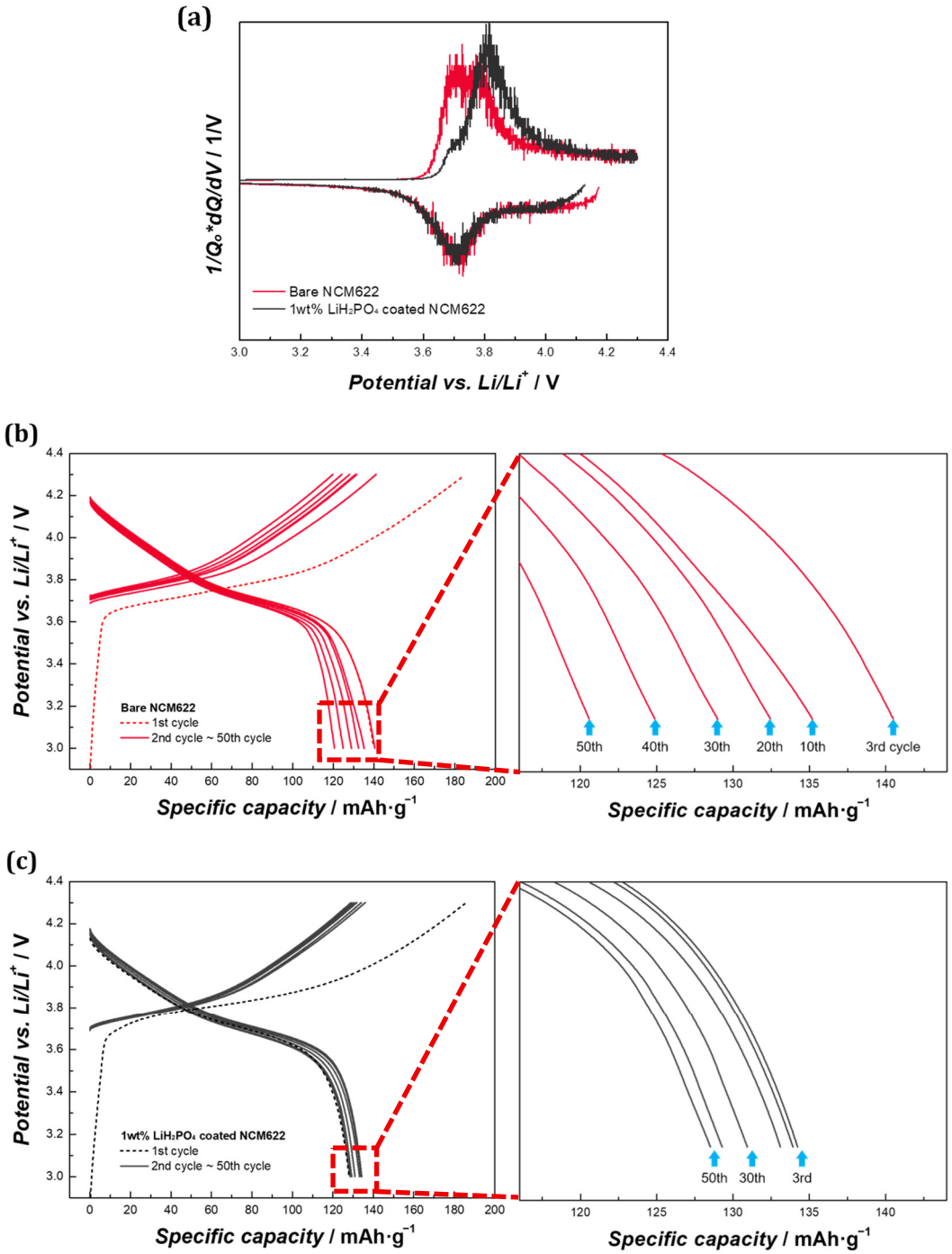


Figure 3. Electrochemical behavior of bare NCM622 and LDP@NCM622. (**a**) First-cycle differential capacity (dQ/dV) curves. Charge–discharge voltage profiles during prolonged cycling of (**b**) NCM622 and (**c**) LDP@NCM622.

The beneficial role of this interphase becomes increasingly evident during prolonged cycling. Figure 3b,c compare the evolution of the charge–discharge voltage profiles with the cycle number. During the initial cycles, LDP@NCM622 exhibits a lower discharge capacity than the bare electrode alongside a slightly larger voltage hysteresis (Figure 3c). This initial capacity reduction (~10 mAh g^{-1}) and kinetic penalty originate from the higher

interfacial resistance introduced by the ~40 nm thick LDP coating layer prior to complete interfacial stabilization. However, this trend rapidly reversed after the initial activation period. While the bare electrode underwent continuous polarization growth accompanied by progressive capacity loss (Figure 3b), the LDP-coated electrode exhibited relatively stable reversible capacity (Figure 3c). After approximately ten cycles, the voltage profiles became highly stable and remained essentially unchanged throughout the subsequent cycling. This fundamentally different evolution indicated that the initial interfacial reaction occurring on LDP@NCM622 rapidly reached a chemically stable state instead of continuously propagating during cycling. In the bare electrode, direct contact between the oxide cathode and sulfide electrolyte allows persistent electrolyte decomposition, leading to the continuous accumulation of resistive interphase products and progressive impedance growth.

In contrast, it is expected that the LDP coating underwent controlled interfacial reconstruction during the early cycles, generating a stable phosphate-rich artificial interphase that effectively passivated the cathode surface and suppressed chemical degradation. Consequently, although the initial activation of the LDP layer imposes a modest capacity and kinetic trade-off (~10 mAh g^{-1}), it substantially mitigates long-term interfacial deterioration, ultimately outperforming the bare cathode in both capacity retention and voltage stability after 10–15 cycles.

The cycling performance (Figure 4a) provides direct evidence supporting this mechanism. Bare NCM622 retained only 73.9% of its second-cycle discharge capacity after 100 cycles, whereas LDP@NCM622 maintained 94.1% of its capacity, corresponding to an improvement of more than 20 percentage points in capacity retention. Although the phosphate coating slightly sacrificed the initial discharge capacity because of the additional interfacial resistance, its ability to stabilize the cathode–electrolyte interface ultimately delivered a substantially higher reversible capacity after prolonged cycling. These results demonstrate that the effectiveness of an artificial interphase should not be determined solely based on its initial electrochemical response. Rather, the ability to suppress interfacial degradation and stabilize impedance evolution during cycling is a decisive factor governing the long-term performance of sulfide-based ASSBs.

Figure 4b,c show the results of EIS performed after the 51st and 101st cycles in the fully charged state, further elucidating the interfacial evolution during cycling. Measurements under charged conditions are particularly advantageous because the impedance contribution from the cathode–electrolyte interface ($R_{cathode/SE}$) can be clearly separated from that of the grain boundary of the sulfide electrolyte ($R_{G.B.}$) and the anode–electrolyte interface ($R_{Anode/SE}$). The resulting spectra reveal two fundamentally different modes of interfacial evolution. For bare NCM622 (Figures 4b and S4a), $R_{cathode/SE}$ increased markedly between the 51st and 101st charged states, indicating that interfacial decomposition continued throughout cycling. The progressive accumulation of electrochemically inactive decomposition products thickens the reaction layer and impedes Li-ion transport. Because sulfide-derived decomposition products generally have poor ionic conductivity, their continuous growth inevitably increases the charge-transfer resistance and aggravates electrode polarization.

In contrast, LDP@NCM622 exhibited distinctly different impedance evolution (Figures 4c and S4b). Although the $R_{cathode/SE}$ impedance was initially higher than that of the bare electrode after 50 cycles, relatively lower impedance growth was observed during the subsequent 50 cycles. This behavior indicates that the interfacial reaction rapidly becomes self-limiting once a phosphate-rich artificial interphase is established. Accordingly, the relatively high initial resistance should not be taken as evidence of an inferior interface. Rather, it represents the electrochemical signature of a deliberately engineered interphase that remains chemically and electrochemically stable during prolonged cycling. This be-

havior closely resembles the formation mechanism of a solid electrolyte interphase (SEI) on graphite anodes in conventional lithium-ion batteries. Although SEI formation causes an initial increase in the interfacial resistance and irreversible lithium consumption, the resulting passivation layer effectively suppresses further electrolyte decomposition, thereby ensuring long-term electrochemical stability. A similar mechanism appeared to operate in the proposed system. During the initial electrochemical activation, the LiH_2PO_4 coating undergoes controlled interfacial reconstruction through limited chemical interaction with the sulfide electrolyte, producing a stable phosphate-rich interphase. While this process introduces an initial kinetic penalty, it effectively prevents continuous electrolyte decomposition and stabilizes the cathode–electrolyte interface, thereby minimizing impedance growth during extended cycling.

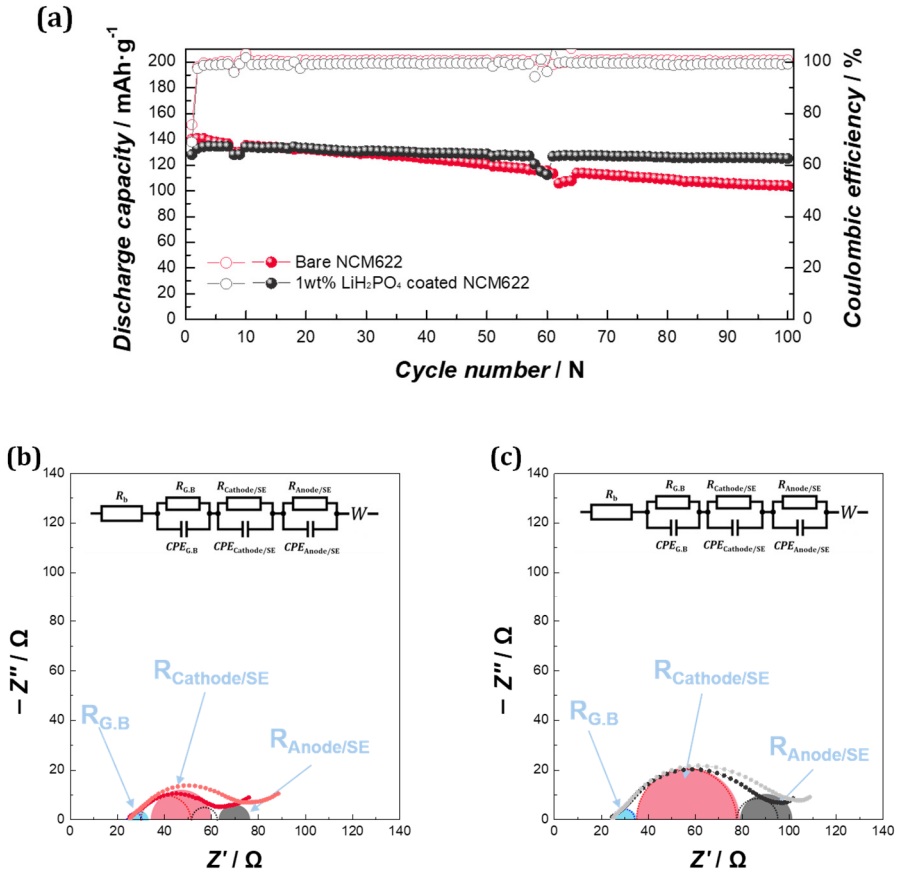


Figure 4. Electrochemical performance and impedance evolution of bare NCM622 and LDP@NCM622. (**a**) Cycling performance and coulombic efficiency measured at 0.22 C. (**b**,**c**) Electrochemical impedance spectra of (**b**) bare NCM622 and (**c**) LDP@NCM622 collected after the 51st and 101st charged states, illustrating the evolution of the cathode–electrolyte interfacial resistance during cycling. The corresponding equivalent circuit model used for impedance fitting is shown in each inset.

Although the electrochemical results clearly demonstrate that the LDP coating effectively suppresses the impedance evolution during cycling, the underlying stabilization mechanism cannot be fully understood without examining the chemical reactions occurring at the cathode–electrolyte interface. To elucidate the evolution of interfacial chemistry, XPS analyses were performed before and after electrochemical cycling. Figure 5 shows a comparison of the S 2p spectra of bare NCM622 and LDP@NCM622. Prior to cycling, the bare electrode (Figure 5a) exhibited the characteristic PS_4^{3-} species (161.3 eV) originating from the argyrodite Li_6PS_5Cl electrolyte [31], along with minor P–$[S]_n$–P (163.2 eV) and S^{2-} components (159.7 eV) [32,33]. These sulfur-deficient species are commonly ob-

served in sulfide electrolytes synthesized at elevated temperatures and arise from the partial volatilization of sulfur during heat treatment. Because the P–S bond is considerably stronger than the Li–S bond, sulfur loss preferentially disrupts the Li–S environment while largely preserving the tetrahedral PS_4^{3-} framework, resulting in the coexistence of reduced sulfur species and sulfur-deficient P–$[S]_n$–P units. Following electrochemical cycling, the interfacial chemistry of the bare electrode changed significantly. New S–S (164.2 eV) and SO_x components (167.5 eV) emerged, providing clear evidence of continuous sulfide electrolyte decomposition. The appearance of oxidized sulfur species is particularly significant because previous studies have shown that oxygen released from highly delithiated layered oxides readily reacts with sulfide electrolytes to form SO_x species [34,35]. Accordingly, the simultaneous formation of S–S and SO_x indicates coupled degradation of both the sulfide electrolyte and the layered oxide cathode, highlighting the absence of an effective interfacial passivation mechanism.

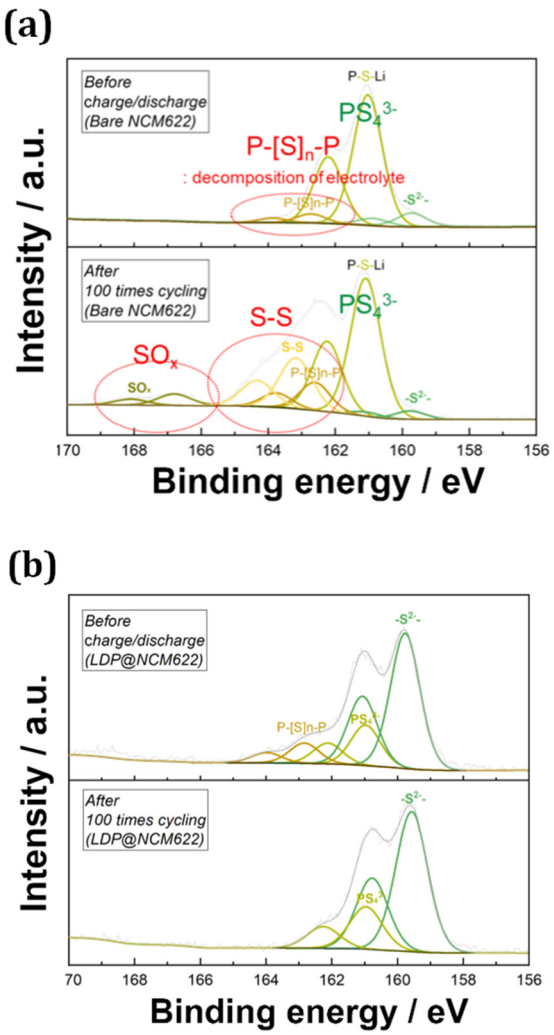


Figure 5. XPS S 2p spectra of (**a**) bare NCM622 and (**b**) LDP@NCM622 before cycling and after 100 cycles, illustrating the evolution of interfacial chemistry induced by the LiH_2PO_4 coating.

A fundamentally different evolution was observed in LDP@NCM622 (Figure 5b). Even before electrochemical cycling, the coated electrode exhibited a substantially stronger S^{2-} component than the bare cathode. Although this initially appeared counterintuitive, a control experiment in which LiH_2PO_4 was simply mixed with Li_6PS_5Cl (Figure S5) provides important insight into the origin of this behavior. Even without electrochemical cycling, direct contact between LiH_2PO_4 and Li_6PS_5Cl resulted in the emergence of a new

phosphate-related P_xO_y component (133.6 eV) together with a pronounced increase in the S^{2-} signal. These observations clearly indicate that LiH_2PO_4 is not chemically inert toward the sulfide electrolyte but instead undergoes an initial chemical reaction upon contact with Li_6PS_5Cl. The concomitant evolution of the phosphate-related P_xO_y component and sulfur species suggests coupled interfacial reactions involving both the phosphate precursor and the sulfide framework. This interpretation is further supported by Figure S6, which shows a substantial decrease in the sulfur-deficient P–$[S]_n$–P component after interfacial reaction with the LDP coating despite the use of the same sulfide electrolyte. Nevertheless, the present XPS results do not establish a direct one-to-one conversion of P–$[S]_n$–P into P_xO_y; rather, they support the formation of a chemically reconstructed, phosphate-rich interfacial environment through the initial reaction between LiH_2PO_4 and Li_6PS_5Cl. Consequently, the relatively high initial interfacial resistance observed in LDP@NCM622 is attributed not simply to the intrinsic ionic resistance of the LiH_2PO_4 layer, but also to the formation of this chemically reconstructed phosphate-rich interphase.

This finding fundamentally revises the conventional view on cathode coatings in sulfide ASSBs. Most oxide coatings are considered chemically inert barriers that prevent direct contact between the cathode and the electrolyte. In contrast, LiH_2PO_4 functions as a chemically active interphase precursor. Rather than completely suppressing the interfacial reactions, it promotes a controlled initial reaction that selectively converts unstable sulfur-deficient species into chemically stable phosphate-containing products. Once this artificial interphase is established, the subsequent reaction pathway fundamentally changes.

After prolonged cycling, the S 2p spectra of LDP@NCM622 differed markedly from those of the bare electrode. Although a small amount of P–$[S]_n$–P species reappeared during cycling, neither sulfur precipitation (S–S) nor oxidized sulfur species (SO_x) were detected. The absence of these decomposition products demonstrates that both continuous sulfide electrolyte degradation and oxygen-induced oxidation reactions were effectively suppressed. Consequently, the phosphate-rich interphase interrupted the coupled degradation of the electrolyte and layered oxide, leading to a chemically stabilized interface.

The interfacial evolution described above also provides a direct explanation of the electrochemical behavior discussed in the previous section. The formation of a phosphate-rich interphase during the initial cycles inevitably introduces an additional Li-ion transport barrier, resulting in a relatively large polarization and interfacial resistance at the beginning of cycling. However, because this interphase rapidly reaches a chemically self-limiting state, further electrolyte decomposition is effectively inhibited, and impedance growth is largely suppressed. In contrast, the initial lower resistance of the bare electrode reflects the absence of a protective interphase rather than a more stable interface. Continuous electrolyte decomposition progressively thickens the reaction layer, ultimately leading to severe impedance growth and rapid capacity fading.

Accordingly, the initial electrochemical penalty associated with LDP should not be considered a drawback but rather as the cost of constructing a chemically stable artificial interface. Once established, this phosphate-rich interphase effectively decouples the layered oxide cathode from the highly reactive sulfide electrolyte while preserving sufficient lithium-ion transport, thereby fundamentally altering the long-term degradation pathway at the cathode–electrolyte interface.

The results of cross-sectional STEM–EDS analyses performed after 100 charge–discharge cycles further elucidate how the modified interfacial chemistry governs long-term electrochemical stability. Figure 6 compares the elemental distributions across the cathode–electrolyte interface for bare NCM622 and LDP@NCM622 after prolonged cycling. As shown in the figure, the elemental distributions remain sufficiently well-resolved to reveal distinct differences in the interfacial evolution. For the bare electrode (Figure 6a), pro-

nounced elemental interdiffusion was observed across the cathode–electrolyte interface. Transition metals originating from the layered oxide, particularly Ni and Co, diffused into the sulfide electrolyte, while sulfur and phosphorus from Li_6PS_5Cl simultaneously penetrated the cathode surface. The resulting interdiffusion region extended to approximately 150 nm from the original interface, demonstrating extensive chemical mixing between the two phases. Such interdiffusion is widely recognized as one of the dominant degradation pathways in sulfide-based ASSBs because it continuously alters the local chemical composition of both the cathode and the electrolyte, promoting the formation of electrochemically inactive products, including transition metal sulfides, lithium phosphates, sulfur-rich species, and mixed oxy-sulfide compounds [12–15]. The progressive accumulation of these poorly ion-conductive products thickens the resistive interphase and ultimately accelerates impedance growth and capacity fading.

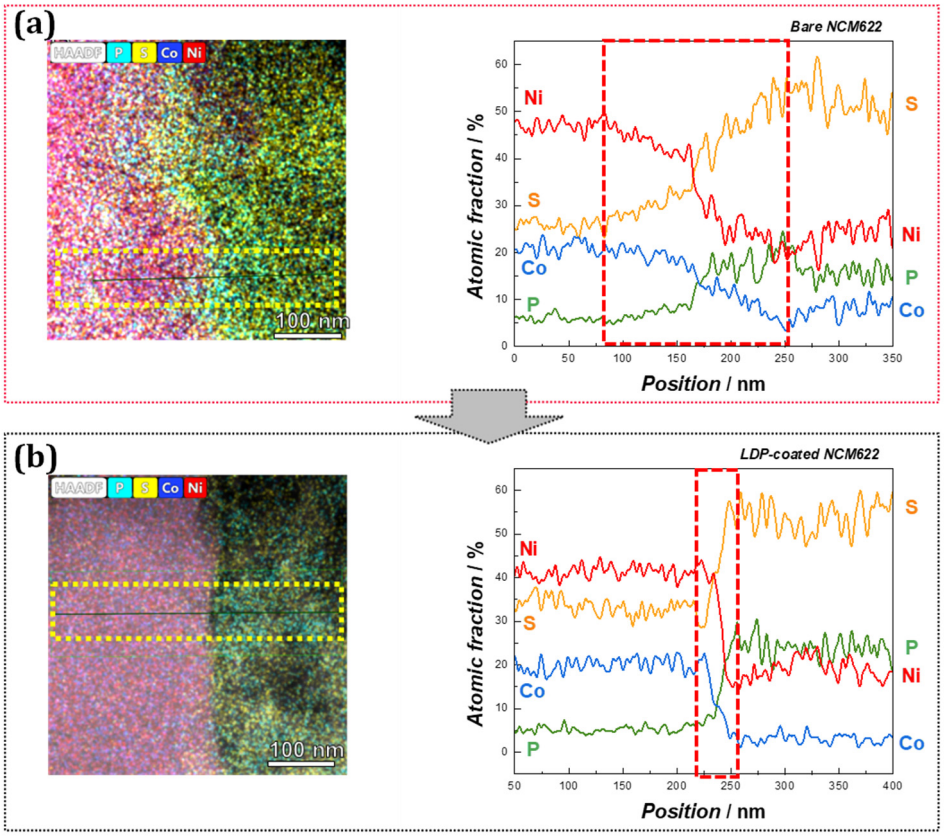


Figure 6. Cross-sectional STEM–EDS elemental mapping of (**a**) bare NCM622 and (**b**) LDP@NCM622 after 100 cycles, showing suppression of elemental interdiffusion and chemical mixing by the LiH_2PO_4-derived artificial interphase.

In contrast, the LDP-coated electrode exhibited a fundamentally different interfacial evolution. As shown in Figure 6b, phosphorus originating from the LDP layer remains confined to the original coating region, whereas the migration of Ni, Co, S, and P across the interface is effectively suppressed. More importantly, no measurable elemental interdiffusion beyond the ~40 nm phosphate layer was detected even after prolonged cycling. These observations demonstrate that the LDP coating continued to function as an effective chemical diffusion barrier despite undergoing partial chemical reconstruction during the initial electrochemical activation.

This behavior provides important insights into the role of phosphate coating. Rather than merely acting as a passive physical barrier, the LDP layer establishes a chemically stabilized interface that substantially reduces the chemical potential gradient that drives

interfacial ion exchange. Once the phosphate-rich artificial interphase is formed, further interdiffusion between the layered oxide cathode and sulfide electrolyte becomes thermodynamically unfavorable, thereby effectively arresting the propagation of the reaction zone. This chemically stabilized interface also explains the negligible impedance growth observed in Figure 4. Because the interfacial reactions become self-limiting after the initial formation process, additional electrochemically inactive decomposition products are no longer continuously generated. Consequently, the thickness and composition of the interphase remain essentially unchanged during prolonged cycling, resulting in a stable charge-transfer resistance and sustained electrochemical performance.

While chemical stability is indispensable for sulfide-based ASSBs, long-term performance also depends critically on preserving the mechanical integrity at the solid–solid interface. Unlike liquid electrolytes, which readily wet newly exposed surfaces, solid electrolytes cannot reestablish intimate contact once interfacial separation occurs. Repeated volume changes in layered oxide cathodes frequently generate interfacial voids that interrupt lithium-ion transport and accelerate electrochemical degradation. Figure 7 shows the results of cross-sectional FIB analyses conducted after 100 cycles; these help examine whether the LDP-derived interphase also contributed to mechanical stabilization.

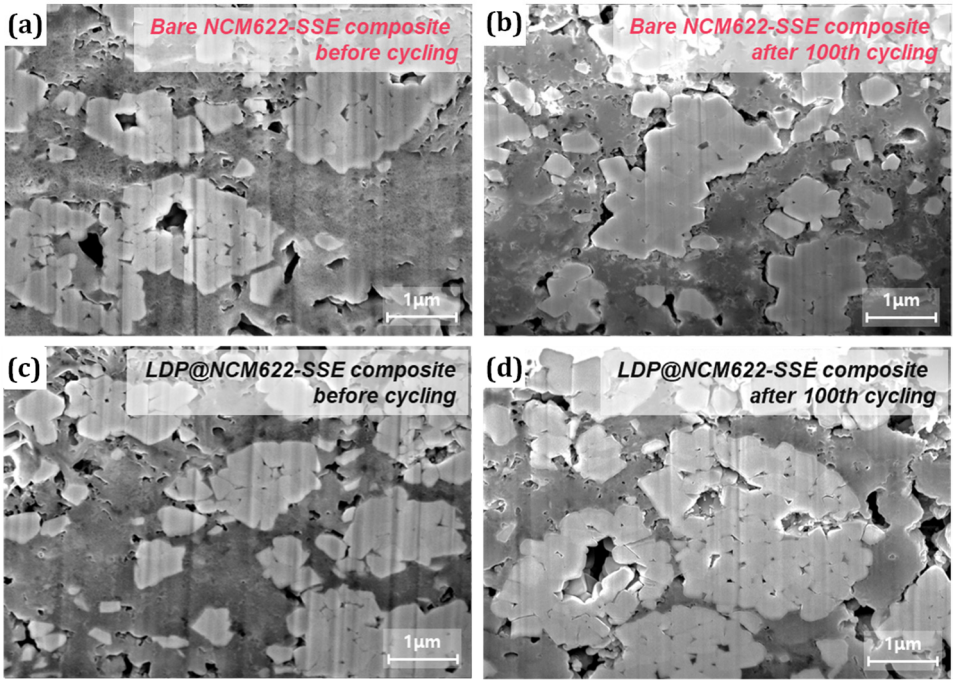


Figure 7. Cross-sectional FIB–SEM images of (**a**) bare NCM622 before cycling, (**b**) bare NCM622 after 100 charge–discharge cycles, (**c**) LDP@NCM622 before cycling, and (**d**) LDP@NCM622 after 100 charge–discharge cycles.

The bare NCM622 electrode exhibited numerous voids along the cathode–electrolyte interface after 100 cycles (Figure 7b). Although these voids primarily originate from the repeated volume variation in the cathode during lithiation and delithiation, continuous interfacial side reactions further weaken the structural integrity and promote contact loss [36]. Once local separation occurs, the effective reaction area decreases, leading to current localization in the remaining contact regions. This, in turn, accelerates local electrolyte decomposition and heterogeneous growth of the interphase, establishing a positive feedback loop between chemical degradation and mechanical failure.

Remarkably, LDP@NCM622 exhibited a different behavior. Even after 100 cycles (Figure 7d), the intimate interfacial contact was preserved across almost the entire cathode

surface with negligible void formation. Therefore, the phosphate-derived interphase not only suppresses interfacial reactions but also maintains structural continuity between the cathode and sulfide electrolyte throughout repeated cycling. Because chemical degradation was effectively inhibited, the formation of mechanically fragile reaction products was minimized, allowing stable interfacial contact to be maintained despite repeated electrode volume changes.

Taken together, these results demonstrate that the LDP coating simultaneously enhances the chemical and mechanical stabilities of the cathode–electrolyte interface. Importantly, these two effects are intrinsically coupled. Suppressing chemical degradation prevents the formation of mechanically unstable reaction products, while preserving the intimate interfacial contact minimizes local current concentration and further inhibits electrolyte decomposition. This synergistic stabilization mechanism ultimately accounts for the remarkable cycling stability of LDP-coated cathodes.

4. Conclusions

LiH_2PO_4 was demonstrated to be a low-cost polyanionic coating material capable of fundamentally stabilizing the cathode–electrolyte interface in sulfide-based ASSBs. A uniform phosphate coating was successfully fabricated on NCM622 particles through a scalable spray-drying process without altering the layered crystal structure or particle morphology of the cathode. Unlike conventional oxide coatings that primarily act as chemically inert diffusion barriers, the LiH_2PO_4 layer exhibited a fundamentally different mode of interfacial stabilization. Although the LDP coating introduced a moderate increase in initial interfacial resistance associated with artificial interphase formation, it markedly suppressed subsequent impedance evolution and improved long-term cycling stability, enabling 94.1% capacity retention after 100 cycles compared with 73.9% for the bare cathode. This behavior indicates that the initial resistance increase represents the electrochemical signature of controlled interphase formation rather than a detrimental transport limitation.

XPS analyses revealed that LiH_2PO_4 actively reacts with unstable sulfur-deficient species in the sulfide electrolyte during initial electrochemical activation, forming a phosphate-rich artificial interphase while suppressing reactive P–$[S]_n$–P species. Once established, this chemically equilibrated interface effectively inhibits sulfur precipitation, SO_x formation, and continuous electrolyte decomposition. Cross-sectional STEM–EDS and FIB analyses further demonstrated suppressed elemental interdiffusion and improved preservation of cathode–electrolyte contact during prolonged cycling. These results demonstrate that the LDP-derived interphase simultaneously mitigates chemical degradation and mechanical deterioration, thereby limiting the continuous growth of electrochemically inactive reaction layers.

This study establishes a fundamentally different concept for interface engineering in sulfide-based ASSBs. Rather than functioning as a chemically inert passivation layer, LiH_2PO_4 acts as a chemically active interphase precursor, undergoing a controlled, self-limiting reaction with the sulfide electrolyte to construct a stable phosphate-rich interface. Thus, controlled interfacial reactivity, rather than complete chemical inertness, may represent a more effective strategy for achieving durable cathode–electrolyte interfaces. More broadly, these findings introduce a new design paradigm in which reactive polyanionic compounds serve as self-adaptive artificial interphase precursors, providing a scalable, economically viable, and broadly applicable route toward high-performance sulfide-based ASSBs.

Supplementary Materials: The following supporting information can be downloaded at https://www.mdpi.com/article/10.3390/batteries12090326/s1: Figure S1. X-ray diffraction patterns of LiH_2PO_4 synthesized using different precursor–solvent combinations for selecting the optimal coating solution: Figure S2. X-ray diffraction patterns of pristine LiH_2PO_4 (LDP), bare NCM622, and

LDP-coated NCM622 with different coating contents, confirming preservation of the layered crystal structure after coating: Figure S3. Comparison of the first-cycle differential capacity (dQ/dV) curves of (a) bare NCM622 and (b) LDP@NCM622, highlighting the influence of the LiH_2PO_4 coating on the initial redox behavior: Figure S4. Impedance spectra of (a) bare NCM622 and (b) LDP@NCM622, zoomed in on Rcathode/SE: Figure S5. P 2p XPS spectra of LiH_2PO_4, Li_6PS_5Cl, and their physical mixtures, demonstrating the initial chemical reaction between the phosphate coating and the sulfide electrolyte. The table shows the binding energies and full widths at half maximum (FWHM) of the PxOy peaks for the samples: Figure S6. Enlarged S 2p spectra of LDP@NCM622 excluding the S^{2-} peak, highlighting the change in sulfur-deficient species after interfacial reaction with the sulfide electrolyte.

Author Contributions: Conceptualization, investigation, data curation, writing—original draft preparation, Y.L.; methodology, validation, investigation, visualization, E.C.H.; formal analysis, investigation, data curation, writing—review and editing, Y.J.P.; investigation, supervision, funding acquisition, D.S. All authors have read and agreed to the published version of the manuscript.

Funding: This work was supported by the Materials and Components Technology Development Program (RS-2024-00420247) funded by the Ministry of Trade, Industry & Energy (MOTIE, Korea) and the Korea Planning & Evaluation Institute of Industrial Technology (KEIT). This work was supported by a National Research Foundation of Korea grant funded by the Korean Government (MSIT) (RS-2026-25477002).

Data Availability Statement: Data are contained within the article.

Acknowledgments: This work was supported by the Materials and Components Technology Development Program (RS-2024-00420247) funded by the Ministry of Trade, Industry & Energy (MOTIE, Korea) and the Korea Planning & Evaluation Institute of Industrial Technology (KEIT). This work was supported by a National Research Foundation of Korea grant funded by the Korean Government (MSIT) (RS-2026-25477002).

Conflicts of Interest: Authors Youngmin Lee and Dongwook Shin were employed by the company Solivis Inc. The remaining authors declare that the research was conducted in the absence of any commercial or financial relationships that could be construed as a potential conflict of interest.

References

1. Mach, A.; Morant, C.; Marquez, F. Advancements and challenges in solid-state battery technology: An in-depth review of solid electrolytes and anode innovations. *Batteries* **2024**, *10*, 29. [CrossRef]
2. Biçer, E.; Aksöz, A.; Bakar, R.; Odabaşı, Ç.; Vonk, W.; Soares, M.I.; Gonçalves, R.; Lourenço, E.; Uzel, A.; Aksoy, T.; et al. Solid-State Batteries: Chemistry, Battery, and Thermal Management System, Battery Assembly, and Applications—A Critical Review. *Batteries* **2025**, *11*, 212. [CrossRef]
3. Nguyen, L.H.B.; Broux, T.; Sanz Camacho, P.; Denux, D.; Bourgeois, L.; Belin, S.; Iadecola, A.; Fauth, F.; Carlier, D.; Olchowka, J.; et al. Stability in Water and Electrochemical Properties of the $Na_3V_2(PO_4)_2F_3$–$Na_3(VO)_2(PO_4)_2F$ Solid Solution. *Energy Storage Mater.* **2019**, *20*, 324–334. [CrossRef]
4. Parab, S.; Lee, J.; Miyagishima, M.; Miao, Q.; Bhamwala, B.; Liu, A.; Ah, L.; Sreenarayanan, B.; Ryu, K.; Li, M.; et al. Quantitative Insights for Diagnosing Performance Bottlenecks in Lithium–Sulfur Batteries. *Energy Environ. Sci.* **2025**, *18*, 6283–6296. [CrossRef]
5. Bouguern, M.D.; Ningappa, N.G.; Vishweswariah, K.; Kumar M R, A.; Kanno, R.; Zaghib, K. Comparative Advances in Sulfide and Halide Electrolytes for Commercialization of All-Solid-State Lithium Batteries. *Adv. Mater.* **2026**, *38*, e13255. [CrossRef]
6. Cho, S.-P.; Hameed, M.U.; Hsieh, C.-T.; Liu, W.-R. Interface Engineering of NCMA Cathodes with LATP Coatings for High-Performance Solid-State Lithium Batteries. *Nanomaterials* **2025**, *15*, 1057. [CrossRef]
7. Man, B.; Zeng, Y.; Liu, Q.; Chen, Y.; Li, X.; Luo, W.; Zhang, Z.; He, C.; Jie, M.; Liu, S. A Comprehensive Review of Sulfide Solid-State Electrolytes: Properties, Synthesis, Applications, and Challenges. *Crystals* **2025**, *15*, 492. [CrossRef]
8. Liu, T.; Wang, W.; Liu, W.; Xu, H.; Wu, J. Recent Progress and Perspectives of Li-Argyrodite Sulfide Electrolytes: From Fundamental Mechanisms to Practical All-Solid-State Lithium Batteries. *Inorganics* **2026**, *14*, 125. [CrossRef]
9. Sundar, A.; Kim, T.; Lagunas, F.; Mane, A.U.; Eze, U.D.; Ginter, C.; Pathak, R.; Tepavcevic, S.; Elam, J.W.; Hood, Z.D.; et al. Computationally-Guided Development of Sulfide Solid Electrolyte Powder Coatings for Enhanced Stability and Performance of Solid-State Batteries. *Adv. Sci.* **2025**, *12*, e13191. [CrossRef]

10. Lu, Z.; Li, S.; Li, L.; Ming, L.; Jiang, Z.; Deng, M.; Wang, Z.; Liu, C.; Yu, C. A Fluoride-Incorporated Composite Electrolyte Enabling High-Voltage All-Solid-State Sulfide-Based Lithium Batteries. *J. Mater. Chem. A* **2025**, *13*, 20477–20487. [CrossRef]
11. Roh, J.; Do, N.; Lee, H.; Lee, S.; Pyun, J.; Hong, S.-T.; Chae, M.S. Towards Practical All-Solid-State Batteries: Structural Engineering Innovations for Sulfide-Based Solid Electrolytes. *Energy Mater.* **2025**, *5*, 500061. [CrossRef]
12. Wang, J.; Zhang, Z.; Ying, H.; Zhang, S.; Tan, H.; Han, G.; Han, W.Q. An Effective Artificial Layer Boosting High-Performance All-Solid-State Lithium Batteries with High Coulombic Efficiency. *J. Mater.* **2022**, *8*, 257–265. [CrossRef]
13. Banerjee, A.; Wang, X.; Fang, C.; Wu, E.A.; Meng, Y.S. Interfaces and Interphases in All-Solid-State Batteries with Inorganic Solid Electrolytes. *Chem. Rev.* **2020**, *120*, 6878–6933. [CrossRef]
14. Xu, L.; Tang, S.; Cheng, Y.; Wang, K.; Liang, J.; Liu, C.; Cao, Y.-C.; Wei, F.; Mai, L. Interfaces in Solid-State Lithium Batteries. *Joule* **2018**, *2*, 1991–2015. [CrossRef]
15. Wu, Z.; Li, X.; Zheng, C.; Fan, Z.; Zhang, W.; Huang, H.; Gan, Y.; Xia, Y.; He, X.; Tao, X.; et al. Interfaces in Sulfide Solid Electrolyte-Based All-Solid-State Lithium Batteries: Characterization, Mechanism and Strategy. *Electrochem. Energy Rev.* **2023**, *6*, 10. [CrossRef]
16. Gao, X.; Zhen, Z.; Chen, J.; Xu, R.; Zeng, X.; Su, J.; Chen, Y.; Chen, X.; Cui, L. Interface Stability of Cathode for All-Solid-State Lithium Batteries Based on Sulfide Electrolyte: Current Insights and Future Directions. *Chem. Eng. J.* **2024**, *491*, 152010. [CrossRef]
17. Wang, J.; Wang, C.; Shi, H.; Wang, Z.; Wang, Z.; Li, J.; Chen, X.; Gao, Y.; Bai, Z.; Yan, X. Enabling Superior Cathode/Sulfide Electrolyte Interfacial Stability by Li_3BO_3 Coating for All-Solid-State Li Battery. *J. Mater. Sci.* **2024**, *59*, 20671–20685. [CrossRef]
18. Jung, S.H.; Oh, K.; Nam, Y.J.; Oh, D.Y.; Brüner, P.; Kang, K.; Jung, Y.S. Li_3BO_3–Li_2CO_3: Rationally Designed Buffering Phase for Sulfide All-Solid-State Li-Ion Batteries. *Chem. Mater.* **2018**, *30*, 8190–8200. [CrossRef]
19. Chang, X.; Weng, W.; Li, M.; Wu, M.; Chen, G.Z.; Fow, K.L.; Yao, X. $LiAlO_2$-Modified Li Negative Electrode with $Li_{10}GeP_2S_{12}$ Electrolytes for Stable All-Solid-State Lithium Batteries. *ACS Appl. Mater. Interfaces* **2023**, *15*, 21179–21186. [CrossRef]
20. Walther, F.; Strauss, F.; Wu, X.; Mogwitz, B.; Hertle, J.; Sann, J.; Rohnke, M.; Brezesinski, T.; Janek, J. The Working Principle of a Li_2CO_3/$LiNbO_3$ Coating on NCM for Thiophosphate-Based All-Solid-State Batteries. *Chem. Mater.* **2021**, *33*, 2110–2125. [CrossRef]
21. Payandeh, S.; Strauss, F.; Mazilkin, A.; Kondrakov, A.; Brezesinski, T. Tailoring the $LiNbO_3$ Coating of Ni-Rich Cathode Materials for Stable and High-Performance All-Solid-State Batteries. *Nano Res. Energy* **2022**, *1*, e9120016. [CrossRef]
22. Lim, C.B.; Park, Y.J. Precursor-Based Surface Modification of Cathodes Using Ta and W for Sulfide-Based All-Solid-State Batteries. *Sci. Rep.* **2020**, *10*, 10501. [CrossRef]
23. Strauss, F.; Teo, J.H.; Maibach, J.; Kim, A.-Y.; Mazilkin, A.; Janek, J.; Brezesinski, T. Li_2ZrO_3-Coated NCM622 for Application in Inorganic Solid-State Batteries: Role of Surface Carbonates in the Cycling Performance. *ACS Appl. Mater. Interfaces* **2020**, *12*, 57146–57154. [CrossRef]
24. Kim, Y.J.; Rajagopal, R.; Kang, S.; Ryu, K.S. Novel Dry Deposition of $LiNbO_3$ or Li_2ZrO_3 on $LiNi_{0.6}Co_{0.2}Mn_{0.2}O_2$ for High Performance All-Solid-State Lithium Batteries. *Chem. Eng. J.* **2020**, *386*, 123975. [CrossRef]
25. Lee, J.Y.; Noh, S.; Seong, J.Y.; Lee, S.; Park, Y.J. Suppressing Unfavorable Interfacial Reactions Using Polyanionic Oxides as Efficient Buffer Layers: Low-Cost Li_3PO_4 Coatings for Sulfide-Electrolyte-Based All-Solid-State Batteries. *ACS Appl. Mater. Interfaces* **2023**, *15*, 12998–13011. [CrossRef]
26. Sakuda, A.; Hayashi, A.; Tatsumisago, M. Interfacial Observation between $LiCoO_2$ Electrode and Li_2S-P_2S_5 Solid Electrolytes of All-Solid-State Lithium Secondary Batteries Using Transmission Electron Microscopy. *Chem. Mater.* **2010**, *22*, 949–956. [CrossRef]
27. Xiao, Y.; Miara, L.J.; Wang, Y.; Ceder, G. Computational Screening of Cathode Coatings for Solid-State Batteries. *Joule* **2019**, *3*, 1252–1275. [CrossRef]
28. Ma, Y.; Pan, B.; Zhao, J.; Chen, C.; Liu, S.; Zheng, Q.; Hu, Y.; Zhang, Y. A Dual-Function LiH_2PO_4 Coating via Residual Lithium Conversion for High-Performance $LiNi_{0.83}Co_{0.12}Mn_{0.05}O_2$ Cathodes. *Mater. Today Energy* **2026**, *59*, 102310. [CrossRef]
29. Chen, Y.; Wang, L.; He, H.; Li, J.; Li, Y.; Liu, R.; Li, D.; He, Z. Preparation of $FePO_4$ and LiH_2PO_4 from Cathode Mixture Materials of Scrapped $LiFePO_4$ Batteries. *J. Mater. Sci. Mater. Electron.* **2020**, *31*, 4083–4091. [CrossRef]
30. Fang, A.; Jia, X. Functional Cathode Coatings of LiH_2PO_4 and $LiTi_2(PO_4)_3$ for Solid-State Batteries. *J. Electrochem. Energy Convers. Storage* **2022**, *19*, 021011. [CrossRef]
31. Kim, A.-Y.; Strauss, F.; Bartsch, T.; Teo, J.H.; Hatsukade, T.; Mazilkin, A.; Janek, J.; Hartmann, P.; Brezesinski, T. Stabilizing Effect of a Hybrid Surface Coating on a Ni-Rich NCM Cathode Material in All-Solid-State Batteries. *Chem. Mater.* **2019**, *31*, 9664–9672. [CrossRef]
32. Zhang, W.; Leichtweiß, T.; Culver, S.P.; Koerver, R.; Das, D.; Weber, D.A.; Zeier, W.G.; Janek, J. The Detrimental Effects of Carbon Additives in $Li_{10}GeP_2S_{12}$-Based Solid-State Batteries. *ACS Appl. Mater. Interfaces* **2017**, *9*, 35888–35896. [CrossRef]
33. Joo, M.J.; Kim, M.; Chae, S.; Ko, M.; Park, Y.J. Additive-Derived Surface Modification of Cathodes in All-Solid-State Batteries: The Effect of Lithium Difluorophosphate- and Lithium Difluoro(oxalato)borate-Derived Coating Layers. *ACS Appl. Mater. Interfaces* **2023**, *15*, 59389–59402. [CrossRef]

34. Jung, S.-K.; Kim, H.; Song, S.H.; Lee, S.; Kim, J.; Kang, K. Unveiling the Role of Transition-Metal Ions in the Thermal Degradation of Layered Ni–Co–Mn Cathodes for Lithium Rechargeable Batteries. *Adv. Funct. Mater.* **2022**, *32*, 2108790. [CrossRef]
35. Koerver, R.; Zhang, W.; de Biasi, L.; Schweidler, S.; Kondrakov, A.O.; Kolling, S.; Brezesinski, T.; Hartmann, P.; Zeier, W.G.; Janek, J. Chemo-Mechanical Expansion of Lithium Electrode Materials—On the Route to Mechanically Optimized All-Solid-State Batteries. *Energy Environ. Sci.* **2018**, *11*, 2142–2158. [CrossRef]
36. Han, Y.; Jung, S.H.; Kwak, H.; Jun, S.; Kwak, H.H.; Lee, J.H.; Hong, S.-T.; Jung, Y.S. Single- or Poly-Crystalline Ni-Rich Layered Cathode, Sulfide or Halide Solid Electrolyte: Which Will Be the Winners for All-Solid-State Batteries? *Adv. Energy Mater.* **2021**, *11*, 2100126. [CrossRef]

Disclaimer/Publisher's Note: The statements, opinions and data contained in all publications are solely those of the individual author(s) and contributor(s) and not of MDPI and/or the editor(s). MDPI and/or the editor(s) disclaim responsibility for any injury to people or property resulting from any ideas, methods, instructions or products referred to in the content.